Q-switching stability limits of continuous-wave passive mode locking

C. Hönninger, R. Paschotta, F. Morier-Genoud, M. Moser, and U. Keller

Ultrafast Laser Physics, Institute of Quantum Electronics, Swiss Federal Institute of Technology, ETH Hönggerberg-HPT, CH-8093 Zürich, Switzerland

Received August 18, 1998; revised manuscript received September 28, 1998

The use of a saturable absorber as a passive mode locker in a solid-state laser can introduce a tendency for *Q*-switched mode-locked operation. We have investigated the transition between the regimes of cw mode locking and *Q*-switched mode locking. Experimental data from Nd:YLF lasers in the picosecond domain and soliton mode-locked Nd:glass lasers in the femtosecond domain, both passively mode locked with semiconductor saturable absorber mirrors, were compared with predictions from an analytical model. The observed stability limits for the picosecond lasers agree well with a previously described model, while for soliton mode-locked femtosecond lasers we have developed an extended theory that takes into account nonlinear soliton-shaping effects and gain filtering. © 1999 Optical Society of America [S0740-3224(99)01001-2]

OCIS codes: 140.3580, 140.4050, 140.3540, 140.7090.

1. INTRODUCTION

Solid-state lasers can be passively mode locked by incorporation of a saturable absorber, which, however, at the same time introduces a *Q*-switching tendency that can drive the laser into the regime of *Q*-switched mode locking (QML).[1,2] In this regime of operation the laser output consists of mode-locked pulses underneath a *Q*-switched envelope (Fig. 1 below). The mode-locked pulse repetition rate is typically of the order of 100 MHz, determined by the laser cavity length, while typical *Q*-switching modulations have frequencies in the kilohertz region. These *Q*-switching instabilities are unwanted for many applications in which constant pulse energy and high repetition rate are required. However, for some applications, such as nonlinear frequency conversion, precise fabrication of microstructures,[3] or surgery,[4] the QML regime may be attractive because of the significantly increased pulse energy that is still concentrated in ultrashort mode-locked pulses. In any case, it is important to understand the solid-state laser dynamics with respect to QML to suppress or exploit this mode of operation.

For a long time QML was always observed when solid-state lasers with long upper-state lifetimes (i.e., longer than one microsecond) have been passively mode locked with an intracavity saturable absorber.[1] Early examples are ruby lasers[5] with dye and color-filter glass saturable absorbers and Nd:glass lasers[6] with dye saturable absorbers. *Q*-switching instabilities could not be suppressed in solid-state lasers because of the limited parameter regime of available saturable absorbers used in the past. The first intracavity saturable absorber that generated stable self-starting cw mode-locked pulses from a solid-state laser with a long upper-state lifetime was based on semiconductor nonlinearities.[7] Since then, many different lasers have been successfully mode locked with excellent stability.[8,9] Semiconductor saturable absorbers have the advantage that the relevant absorber parameters can be varied by several orders of magnitude. Therefore semiconductor saturable absorbers offer significant improvements in performance compared with other saturable absorbers used in the past. In addition, the large saturable absorber parameter range allowed for a systematic investigation of the *Q*-switching stability limits in passively mode-locked solid-state lasers. The first analytical treatment of QML in solid-state lasers mode locked by saturable absorbers was done by Kärtner *et al.*[2]; experiments with a semiconductor saturable absorber mode-locked Nd:YLF laser showed the expected behavior. However, a full quantitative confirmation of the theory was not possible because of the relatively large uncertainty of the absorber parameters.

In this paper we experimentally demonstrate results that are in excellent agreement with the QML threshold as predicted by Kärtner *et al.*[2] in the picosecond pulse regime. In addition, we provide a much simpler and experimentally confirmed stability criterion with easily accessible experimental parameters. For the femtosecond pulse regime we had to extend the theory provided by Kärtner *et al.* to explain the observed significantly higher stability against QML. Therefore this paper is organized as follows. In Section 2 we summarize the theory as developed in Ref. 2, from which we derive a simple stability criterion. Then we extend the model for application to femtosecond lasers, where we demonstrate that the interplay of soliton-shaping effects, gain filtering, and filter effects in the semiconductor saturable absorber increases the stability against QML. In Section 3 we describe the experiments, which were in good agreement with the theory. Finally, we draw conclusions from the obtained results.

2. THEORY

A. Review of the Theory for Picosecond Lasers

In this section we review the theory developed by Kärtner *et al.*,[2] which has been confirmed to be very accurate for

picosecond lasers, and introduce the notation used below. Figure 1 illustrates qualitatively the two laser-operation regimes of interest. The instantaneous laser power is shown versus time. In the cw mode-locking regime [Fig. 1(a)] the laser generates a train of mode-locked pulses with high amplitude stability, while QML [Fig. 1(b)] means that the pulse energy is modulated with a strongly peaked Q-switching envelope. To derive a stability criterion against QML we start from the rate equations for the intracavity power, gain, and saturable absorption. We obtain this criterion by performing a linearized stability analysis analogous to the derivation of the Q-switching criterion for a continuously running laser described in Ref. 1. Stability means that the relaxation oscillations are damped. The rate equations for the mode-locked laser can be written as

$$\frac{dP}{dt} = \frac{g - l - q_P(E_P)}{T_R} P, \tag{1}$$

$$\frac{dg}{dt} = -\frac{g - g_0}{\tau_L} - \frac{P}{E_{\mathrm{sat},L}} g, \tag{2}$$

$$\frac{dq}{dt} = -\frac{q - q_0}{\tau_A} - \frac{P}{E_{\mathrm{sat},A}} q, \tag{3}$$

where P is the average intracavity laser power and T_R the cavity round-trip time. $E_P = PT_R$ is the energy of a mode-locked pulse in the cavity. We always assume fundamental mode locking, i.e., the presence of a single pulse in the cavity. g and q are the time-dependent round-trip power gain and the saturable absorption coefficient, respectively, while g_0 and q_0 denote the corresponding quantities in equilibrium with no intracavity power, i.e., for $P = 0$. l is the linear loss per round trip. The quantities g, l, and q are defined with respect to the laser power, not the field amplitude as in Ref. 2. Note that the quantities P, E_P, and g are described on the time scale of several round-trip times T_R, whereas Eq. (3) for $q(t)$ must be solved for the time elapsed during a pulse. τ_L and τ_A are the upper-state lifetime of the laser medium and the absorber recovery time, respectively.

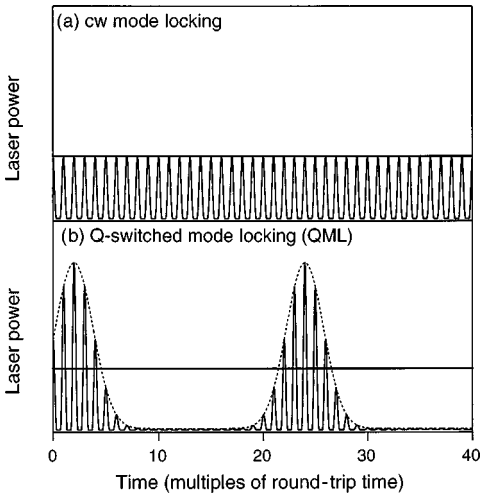

Fig. 1. Instantaneous and average laser power versus time for (a) a stable cw mode-locked laser and for (b) a mode-locked laser exhibiting large Q-switching instabilities. The average laser power (thick line) is the same for both lasers.

$E_{\mathrm{sat},L}$ is the saturation energy of the gain, which is defined as the product of saturation fluence $F_{\mathrm{sat},L} = h\nu/(m\sigma_L)$ and the effective laser mode area inside the gain medium $A_{\mathrm{eff},L}$. We define the effective mode area as $A_{\mathrm{eff},L} = \pi w^2$, where w is the $1/e^2$ Gaussian beam radius with respect to intensity. The factor m in the definition of $F_{\mathrm{sat},L}$ is the number of passes through the gain element per cavity round trip. Because of this factor, the gain saturation depends on the geometry of the laser cavity. For a ring cavity, $m = 1$, while for a simple standing-wave cavity $m = 2$. For a cavity with multiple passes through the gain medium, m can be larger than 2. For simplicity, we assume the gain material to be homogeneously broadened. Note, however, that inhomogeneous line broadening, e.g., in laser glasses, also influences the saturation behavior of the gain. The measured emission cross section σ_L at a certain wavelength usually represents an average for all ions. However, the laser ions with the largest cross sections participate more strongly in the Q-switching cycle, so the gain saturation is stronger than that assumed by use of the averaged cross section; as we show below, this should lead to a weaker tendency for QML as compared with the predictions of our model. We also neglect spatial hole-burning effects, assuming, e.g., that the gain medium is located in the middle of a standing-wave laser cavity.[10,11]

$E_{\mathrm{sat},A}$ denotes the absorber saturation energy and is defined by the product of absorber saturation fluence $F_{\mathrm{sat},A}$ and effective laser mode area on the saturable absorber $A_{\mathrm{eff},A}$. $F_{\mathrm{sat},A}$ can be measured and corresponds to the pulse fluence that is necessary to bleach the saturable absorption to $1/e$ of its maximum amount q_0.

$q_P(E_P)$ in Eq. (1) represents the round-trip loss in average laser power (or pulse energy) introduced by the saturable absorber for a given intracavity pulse energy. We make two assumptions to determine q_P. First, we assume a slow absorber, i.e., the duration τ_P of the mode-locked pulses must be shorter than the absorber recovery time τ_A, although we found that the results remain valid even for $\tau_A \approx \tau_P$ (see Section 3). Second, the absorber recovery time τ_A must be much shorter than the cavity round-trip time T_R. This can easily be achieved for semiconductor absorbers, since τ_A can be custom designed within a wide range.[8] With these assumptions we can neglect the relaxation term in Eq. (3) during the time necessary for a mode-locked pulse to pass the saturable absorber, and we can assume that the absorber is always fully recovered before it is hit by the next pulse. Then, for the pulse energy loss per round trip,[2] we obtain

$$q_P(E_P) = q_0 \frac{F_{\mathrm{sat},A} A_{\mathrm{eff},A}}{E_P} \left[1 - \exp\left(-\frac{E_P}{F_{\mathrm{sat},A} A_{\mathrm{eff},A}}\right)\right]. \tag{4}$$

Using this result, we can describe the mode-locked laser by the following two coupled rate equations:

$$T_R \frac{dE_P}{dt} = [g - l - q_P(E_P)]E_P, \tag{5}$$

$$\frac{dg}{dt} = -\frac{g - g_0}{\tau_L} - \frac{E_P}{E_{\mathrm{sat},L} T_R} g. \tag{6}$$

By linearizing these equations for small deviations δE_P and δg from the steady-state values $\bar{E}_P$ and $\bar{g}$ in analogy to the analysis given in Ref. 1, we obtain the criterion

$$E_P \left| \frac{\mathrm{d}q_P}{\mathrm{d}E_P} \right|_{\bar{E}_P} < \frac{T_R}{\tau_L} r = \frac{T_R}{\tau_L} + \frac{E_P}{E_{\mathrm{sat},L}} \tag{7}$$

for stability against QML.[2] Here we have used $r = 1 + P/P_{\mathrm{sat},L}$. If the absorber is nearly fully saturated, which is normally the case, r is identical to the usual pump parameter that describes how many times above threshold the laser operates.

The physical background of relation (7) can be understood as follows. If the pulse energy rises slightly owing to relaxation oscillations, this pulse energy fluctuation first grows exponentially because of the stronger bleaching of the absorber. However, the increased pulse energy starts to saturate the gain. The laser is stable against QML if the gain saturation is sufficiently strong to stop the exponential rise.

So far, the theory neglects gain filtering and nonlinear effects that act on the pulse bandwidth. This point, however, becomes important for solitonlike pulses in the femtosecond regime. We discuss the consequences of this in Subsection 2.D.

B. Semiconductor Saturable Absorber Mirrors

As passive mode lockers we used semiconductor saturable absorber mirrors (SESAM's), where we integrate the semiconductor saturable absorber directly into a mirror structure, which results in a device whose reflectivity increases as the incident optical intensity increases (Fig. 2). Our SESAM designs, used in this study, correspond to low-finesse antiresonant Fabry–Perot saturable absorbers (A-FPSA's) described in more detail in Refs. 8 and 9.

The nonlinear reflectivity $R(E_P)$ can be measured with the output of another cw mode-locked laser, which provides enough pulse energy to bleach the absorber. The pulse fluence on the absorber can be varied with an adjustable attenuator. A typical nonlinear reflectivity of a SESAM is shown in Fig. 2. The measured data are fitted with the function[12]

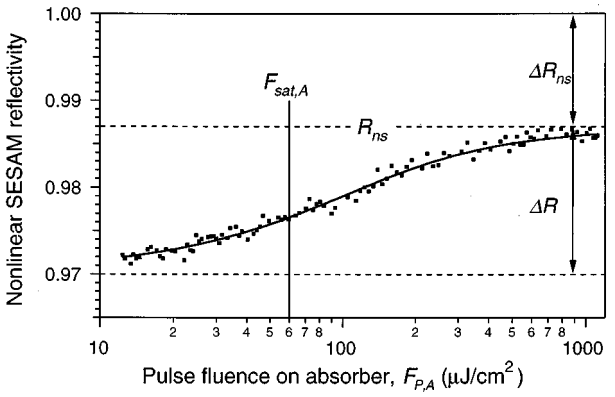

Fig. 2. Measured data (filled points) and fitted (solid) curve according to Eq. (8) for the nonlinear reflectivity $R(F_{P,A})$ at 1047 nm of a SESAM as a function of the pulse energy fluence $F_{P,A} = E_P/A_{\mathrm{eff},A}$. The SESAM parameters are $\Delta R = 1.7\%$, $F_{\mathrm{sat},A} = 60\ \mu\mathrm{J/cm^2}$, $R_{\mathrm{ns}} = 98.7\%$, and $\Delta R_{\mathrm{ns}} = 1.3\%$.

$$R(E_P) = R_{\mathrm{ns}} \frac{\ln\left\{1 + \exp(-\Delta R)\left[\exp\left(\frac{E_P}{E_{\mathrm{sat},A}}\right) - 1\right]\right\}}{E_P/E_{\mathrm{sat},A}}, \tag{8}$$

which was derived from a simple model for nonlinear pulse propagation in the absorber. This is equivalent to the equations used previously.[9,13] The fit parameters are ΔR, $F_{\mathrm{sat},A}$, and R_{ns}. R_{ns} is the reflectivity for high pulse energies and determines the nonsaturable loss $\Delta R_{\mathrm{ns}} = 1 - R_{\mathrm{ns}}$. ΔR is the maximum change in nonlinear reflectivity, which is also referred to as the maximum modulation depth of the SESAM device. For absorbers with ΔR smaller than approximately 10% (as used in all the experiments), we can simplify Eq. (8) to

$$R(E_P) = R_{\mathrm{ns}}\left\{1 - \Delta R \frac{F_{\mathrm{sat},A} A_{\mathrm{eff},A}}{E_P} \times \left[1 - \exp\left(-\frac{E_P}{F_{\mathrm{sat},A} A_{\mathrm{eff},A}}\right)\right]\right\}. \tag{9}$$

The nonlinear reflectivity $R(E_P)$ of the SESAM is related to the pulse energy loss per round trip $q_P(E_P)$. Note that we did not include any nonsaturable losses in $q(t)$ [Eq. (3)] or $q_P(E_P)$ [Eq. (4)]. Therefore the maximum modulation depth is given by $\Delta R = 1 - \exp(-q_0) \approx q_0$ for $\Delta R \ll 1$. For passively mode-locked solid-state lasers we can assume that the modulation depth is small, i.e., $\Delta R \ll 1$. In addition, the nonsaturable losses should be as low as possible because they only degrade the laser performance. For stable mode locking we typically have to use a small output coupler transmission T_{out} of the order of a few percent, which results in the additional condition that $\Delta R_{\mathrm{ns}} \ll T_{\mathrm{out}} \ll 1$. Therefore we can make the approximation that $R_{\mathrm{ns}} \approx 1$ and that

$$R(E_P) \approx \exp[-q_P(E_P)] \approx 1 - q_P(E_P). \tag{10}$$

The approximations made for Eq. (9) are then consistent with Eqs. (10) and (4) by means of $R_{\mathrm{ns}} \approx 1$. The stability criterion against QML from relation (7) can be rewritten with the nonlinear reflectivity as

$$E_P \left. \frac{\mathrm{d}R(E_P)}{\mathrm{d}E_P} \right|_{\bar{E}_P} < \frac{T_R}{\tau_L} r = \frac{T_R}{\tau_L} + \frac{E_P}{E_{\mathrm{sat},L}}. \tag{11}$$

The absorber parameters determine the left-hand side of relation (11), whereas the right-hand side contains the laser material and laser cavity parameters.

C. Simplifications

To benefit from the full modulation depth of the saturable absorber in cw mode-locked lasers, the pulse energy must be high enough to bleach the absorber. To meet that condition, the pulse fluence on the SESAM should be approximately five times the absorber saturation fluence. With this approximation and the assumption that $R_{\mathrm{ns}} = 1$, as well as with relations (10) and (4), we obtain for the nonlinear reflectivity of the SESAM

$$R(E_P) \approx 1 - \Delta R \frac{F_{\mathrm{sat},A} A_{\mathrm{eff},A}}{E_P} \quad \text{or}$$

$$R(F_{P,A}) \approx 1 - \Delta R \frac{F_{\mathrm{sat},A}}{F_{P,A}}, \tag{12}$$

where $F_{P,A} = E_P/A_{\mathrm{eff},A}$ is the pulse fluence (i.e., pulse energy per unit area) incident upon the SESAM. At lower fluences the residual saturable absorption would contribute to the cavity loss and act against self-starting and efficient mode-locked operation.

If the laser operates far above threshold ($r \gg 1$), which is the case in most mode-locked lasers, we can neglect the first term on the right-hand side of relation (11), and the stability criterion against QML becomes independent of the upper-state lifetime of the considered laser material. The saturation energy is then the only relevant parameter of the gain medium. A laser material with a large stimulated-emission cross section σ_L is therefore desirable for stable cw mode locking. It also helps to choose a resonator geometry with multiple passes through the gain medium to decrease the gain saturation fluence. Selecting inhomogeneously broadened gain materials with the same averaged σ_L would also reduce the gain saturation fluence because the class of laser ions with the highest cross sections dominates the gain saturation. Reducing the spontaneous lifetime, e.g., by lifetime quenching effects, does not affect the stability condition against QML.

With the approximations listed above, stability condition (11) can be written in the following equivalent forms:

$$E_P{}^2 > E_{\mathrm{sat},L} E_{\mathrm{sat},A} \Delta R, \tag{13}$$

$$F_{P,A}{}^2 > F_{\mathrm{sat},L} F_{\mathrm{sat},A} \Delta R \frac{A_{\mathrm{eff},L}}{A_{\mathrm{eff},A}}, \tag{14}$$

$$P^2 > F_{\mathrm{sat},L} F_{\mathrm{sat},A} \Delta R A_{\mathrm{eff},L} A_{\mathrm{eff},A} \frac{1}{T_R{}^2}. \tag{15}$$

With respect to the experimental verification of the theory, it is helpful to introduce the QML parameter $E_{\mathrm{sat},L}E_{\mathrm{sat},A}\Delta R$, because it contains all the parameters that determine the laser dynamics. We then define the critical intracavity pulse energy $E_{P,c}$ as the square root of the QML parameter:

$$\begin{aligned} E_{P,c} &\equiv (E_{\mathrm{sat},L} E_{\mathrm{sat},A} \Delta R)^{1/2} \\ &= (F_{\mathrm{sat},L} A_{\mathrm{eff},L} F_{\mathrm{sat},A} A_{\mathrm{eff},A} \Delta R)^{1/2}. \end{aligned} \tag{16}$$

This is the minimum intracavity pulse energy, which is required for obtaining stable cw mode locking; i.e., for $E_P > E_{P,c}$ we obtain stable cw mode locking, and for $E_P < E_{P,c}$ we obtain QML.

Note that, if we neglect the lifetime-dependent term in relation (11) and set the bracketed term in Eq. (9) as 1, both approximations lead to a slightly stricter stability criterion: A laser fulfilling the stability condition with these approximations will always fulfill the exact condition. For good stability of a mode locked laser against unwanted fluctuations of pulse energy, operation close to the stability limit [relations (13)–(16)] is not recommended.

D. Extensions for Soliton Mode-Locked Lasers

We show in Section 3 that the experimental results for a Nd:YLF laser are in good agreement with the theory outlined above. When we checked experimental results from various other passively mode-locked solid-state lasers, we found a similar agreement for other picosecond lasers. However, we discovered that Nd:glass[14] and Yb:glass[15] femtosecond soliton mode-locked lasers[16,17] show stable cw mode locking in a regime in which they should actually be *Q*-switched mode locked according to criterion (11). We explain this below by the interplay of soliton effects and gain filtering. Additionally, there could be effects caused by the saturable absorber, namely, stronger saturation of the fast component[18] for fluctuations toward higher pulse energies (increasing the tendency toward QML), or spectral filtering effects in the bleached SESAM. However, at least in the experiments discussed in this paper, we believe that the previously mentioned interplay of soliton effects and gain filtering dominates.

The basic idea is as follows: If the energy of an ultrashort pulse rises slightly because of relaxation oscillations, self-phase modulation and/or self-amplitude modulation broadens the pulse spectrum. A broader spectrum, however, reduces the effective gain because of the finite gain bandwidth, which provides some negative feedback and thus decreases the critical pulse energy that is necessary for stable cw mode locking.

For a quantitative description of this idea we modify rate equations (5) and (6) by introducing the effective gain for a mode-locked laser running with a spectral distribution $I(\nu)$,

$$g_{\mathrm{eff}} \equiv \frac{\int g(\nu) I(\nu) \mathrm{d}\nu}{\int I(\nu) \mathrm{d}\nu}. \tag{17}$$

$g(\nu)$ describes the gain spectrum of the laser material. If we assume that the pulse spectrum adapts quickly to changes in E_P (i.e., within a time that is much shorter than the period of the relaxation oscillations), we can write g_{eff} as a function of E_P without depending on the history of the pulse. To derive an analytical expression for the effective gain we assume Gaussian-shaped gain and pulse spectra. If we further assume that the pulse spectrum is centered at the peak of the gain spectrum, we obtain for the effective gain

$$g_{\mathrm{eff}}(E_P) = \frac{g}{\left\{1 + \left[\frac{\Delta\nu(E_P)}{\Delta\nu_g}\right]^2\right\}^{1/2}}. \tag{18}$$

$\Delta\nu(E_P)$ and $\Delta\nu_g$ are the full width at half-maximum (FWHM) values of the pulse and the gain spectra, respectively. This results in the following modified set of rate equations:

$$T_R \frac{\mathrm{d}E_P}{\mathrm{d}t} = [g_{\mathrm{eff}}(E_P) - l - q_P(E_P)]E_P, \tag{19}$$

$$\frac{\mathrm{d}g}{\mathrm{d}t} = -\frac{g - g_0}{\tau_L} - \frac{E_P}{E_{\mathrm{sat},L} T_R} g_{\mathrm{eff}}(E_P). \tag{20}$$

From a linearized stability analysis for these rate equations (analogous to the procedure described above and in Ref. 1) we can derive a new condition for stable cw mode-locked operation:

$$E_P\left[\frac{\mathrm{d}g_{\mathrm{eff}}(E_P)}{\mathrm{d}E_P}-\frac{\mathrm{d}q_P(E_P)}{\mathrm{d}E_P}\right]\Bigg|_{\bar{E}_P}<\frac{T_R}{\tau_L}+\frac{E_P}{E_{\mathrm{sat},L}}\frac{g_{\mathrm{eff}}}{g}. \tag{21}$$

With the approximations discussed in Subsection 2.C, which are usually well fulfilled in femtosecond solid-state lasers as well, we can simplify this expression to

$$\left(\frac{g_{\mathrm{eff}}}{g}-\frac{\mathrm{d}g_{\mathrm{eff}}}{\mathrm{d}E_P}\right)\Bigg|_{\bar{E}_P}E_P{}^2>E_{\mathrm{sat},L}E_{\mathrm{sat},A}\Delta R. \tag{22}$$

Relation (22) is a generalization of condition (13). The only modification is the parenthetical term on the left-hand side, which contains gain filtering and spectral broadening effects in the laser. From Eq. (18) we can see that $g_{\mathrm{eff}}/g<1$ and $\mathrm{d}g_{\mathrm{eff}}/\mathrm{d}E_P<0$. The term g_{eff}/g alone would shift the stability limit to higher pulse energies, while the term $\mathrm{d}g_{\mathrm{eff}}/\mathrm{d}E_P$ can significantly increase the magnitude of the parenthetical term on the left-hand side of relation (22) and thus decrease the critical pulse energy substantially (e.g., by a factor of 4; see Section 3). Most picosecond lasers are well described by the simpler relation (13), because the pulse spectra are narrow and the nonlinearities are negligible owing to the low peak intensities. Indeed, we observed no spectral broadening of the pulse bandwidth with increasing pulse energy in our Nd:YLF experiments.

It is convenient to rewrite relation (22) by introducing the new parameter $f\equiv\Delta\nu(E_P)/\Delta\nu_g$, which is the ratio of pulse bandwidth and gain bandwidth. f depends on the pulse energy and on the pulse duration. With $\mathrm{d}g_{\mathrm{eff}}/\mathrm{d}E_P=\mathrm{d}g_{\mathrm{eff}}/\mathrm{d}\Delta\nu\Delta\nu_g\mathrm{d}f/\mathrm{d}E_P$ and Eq. (20), we can rewrite relation (22) as

$$\left[(1+f^2)^{-1/2}+E_{\mathrm{sat},L}gf(1+f^2)^{-3/2}\frac{\mathrm{d}f}{\mathrm{d}E_P}\right]E_P{}^2>E_{\mathrm{sat},L}E_{\mathrm{sat},A}\Delta R. \tag{23}$$

We can now calculate f and $\mathrm{d}f/\mathrm{d}E_P$ from the soliton equation

$$\tau_P=\frac{1.76D_2\lambda_0A_{\mathrm{eff},L}}{4\pi n_2L_K}\frac{1}{E_P} \tag{24}$$

and the constant time–bandwidth product $\Delta\nu\tau_P=0.315$:

$$f=\frac{4\pi n_2L_K}{D_2A_{\mathrm{eff},L}\lambda_0\Delta\nu_g}\frac{0.315}{1.76}E_P, \tag{25}$$

$$\frac{\mathrm{d}f}{\mathrm{d}E_P}=\frac{4\pi n_2L_K}{D_2A_{\mathrm{eff},L}\lambda_0\Delta\nu_g}\frac{0.315}{1.76}\equiv K. \tag{26}$$

Here τ_P is the FWHM soliton duration, λ_0 is the center wavelength of the mode-locked pulse, n_2 is the nonlinear refractive index, and L_K is the propagation length in the Kerr medium per round trip. Usually the gain medium itself acts as the Kerr medium, so in a standing-wave cavity L_K is twice the length of the laser crystal L_g. D_2 denotes the amount of negative intracavity group-delay dispersion (GDD) per round trip, which compensates for the chirp introduced by self-phase modulation. For $f^2=K^2E_P{}^2\ll1$, which is very well fulfilled if the spectrum of the mode-locked pulse fills less than ≈40% of the available gain bandwidth, we can rewrite relation (23) to obtain the more compact form

$$E_{\mathrm{sat},L}gK^2E_P{}^3+E_P{}^2>E_{\mathrm{sat},L}E_{\mathrm{sat},A}\Delta R. \tag{27}$$

3. EXPERIMENTS

A. Picosecond Regime: Nd:YLF

For our picosecond experiments we used Nd:YLF as a crystalline gain material with homogeneous broadening of the optical transition, since we assumed this type of broadening in the theory. We used two different cavity setups (Fig. 3). The first is a standard delta cavity containing a Brewster/Brewster-cut gain medium. The second cavity design is a V cavity, which can be regarded as a delta cavity folded in the middle of the laser crystal. In this experiment we used a flat/Brewster-cut Nd:YLF crystal. The Nd doping of both crystals was 1.5%, resulting in an absorption length of 2.3 mm at a 793-nm pump wavelength. The important laser parameters of Nd:YLF are summarized in Table 1. The crystal lengths are 5 mm for the Brewster/Brewster-cut YLF and 4.5 mm in the center of the flat/Brewster-cut YLF. The laser cavities were designed to reduce spatial hole-burning effects by placement of the gain medium in the middle of the standing-wave resonator[10]; in the V cavity, the overlap volume between the laser modes inside the gain medium was small.

In the experiments with the delta cavity we used a Ti:sapphire laser as a pump source. The maximum power was 1.8 W. At the location of the gain medium we measured a slightly asymmetrical pump radius of 26 μm in the tangential plane and 19 μm in the sagittal plane. The pump mode area was made smaller than the laser mode area inside the gain medium to optimize mode matching and to suppress higher-order transverse modes. The laser mode radii inside the crystal were ≈70 and 50 μm in the tangential and the sagittal planes, respectively, which resulted in an effective laser mode area of $\approx1\times10^{-4}$ cm^2. We achieved mode locking by focusing the laser mode onto the SESAM, using the curved mirror M_3.

To systematically test relations (13)–(16) we varied the significant parameters of the delta cavity, i.e., the cavity round-trip time (T_R) as well as the laser mode areas in the gain medium ($A_{\mathrm{eff},L}$) and on the saturable absorber ($A_{\mathrm{eff},A}$). This is done by means of a change in the ROC of mirror M_3 and by a decrease in the cavity length. The laser mode areas of the different delta cavity setups, which are summarized in Table 2, were calculated with *ABCD* matrix formalism. We varied the cavity round-trip time between ≈5 and 7.4 ns and the laser mode areas on the SESAM between 5×10^{-5} and $\approx4\times10^{-4}$ cm^2. The laser mode areas inside the Nd:YLF crystal varied only slightly among the different delta cavity setups.

The V-cavity Nd:YLF laser [see Fig. 3(b)] was pumped by a Spectra Diode Labs 4-W laser diode operating at 793 nm. The emitting stripe size of the diode was 500 μm in the horizontal plane, resulting in a diode pump beam that was ≈120 times diffraction limited. In the vertical direc-

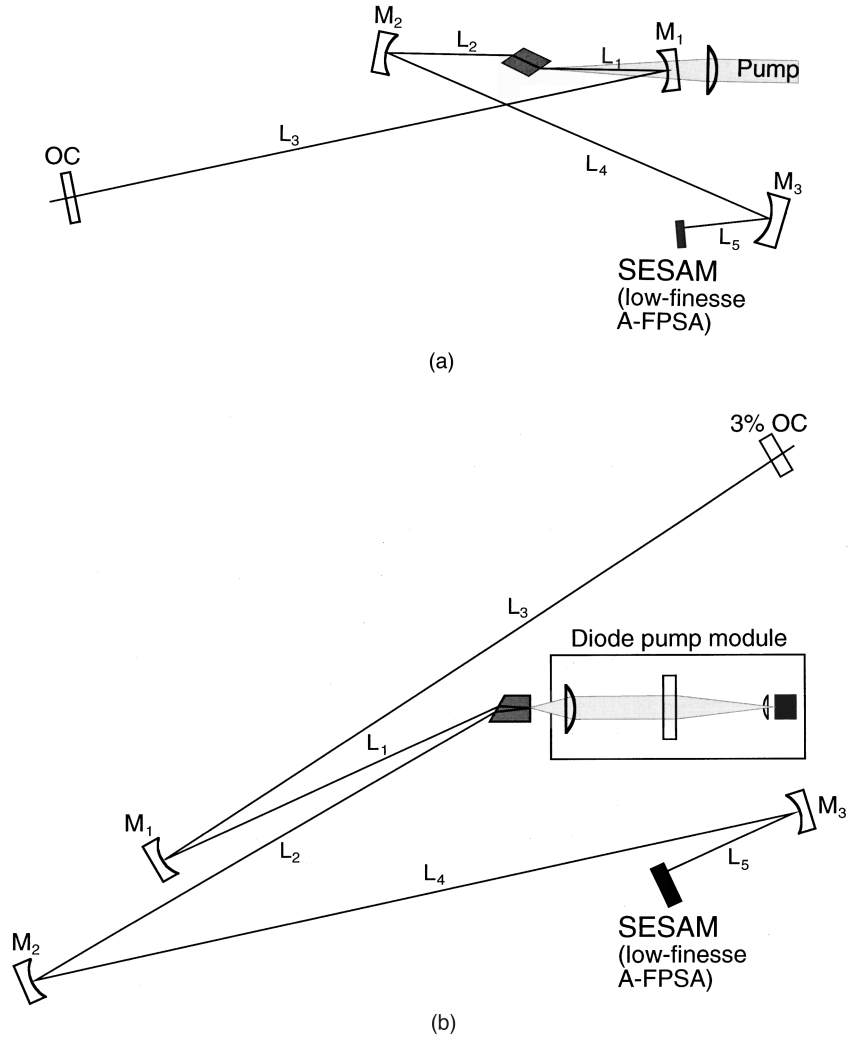

Fig. 3. Nd:YLF laser cavity setups. The parameters for (a) the delta cavity were $M_1 = M_2 = 15$-cm radius of curvature (ROC), $L_1 = 7.6$ cm, $L_2 = 7.9$ cm, $L_3 = 35$ cm, $L_4 = 45$ cm. We used 10-cm-, 15-cm-, and 30-cm-ROC mirrors as M_3, with corresponding lengths (in cm) $L_5 = 4.9, 7.3, 14.3$. We used 0.5%, 1.5%, and 5% output coupling (OC). For the experiment with the higher repetition rate of 197 MHz, M_2 was a 10-cm-ROC mirror and M_3 a 20-cm-ROC mirror. The lengths were $L_1 = 7.5$ cm, $L_2 = 5.4$ cm, $L_3 = 22$ cm, $L_4 = 30$ cm, and $L_5 = 10.6$ cm, and the output coupling was 1%. In (b) the V-cavity laser setup we used 50-cm-, 80-cm-, and 50-cm-ROC mirrors for M_1, M_2, and M_3. The arm lengths were $L_1 = 30.2$ cm, $L_2 = 59.5$ cm, $L_3 = 113$ cm, $L_4 = 90$ cm, and $L_5 = 11.5$ cm. We used a 3% output coupler.

Table 1. Laser Material Parameters[a]

Parameter	Nd(1.5%):YLF	Nd(4%):glass (Schott LG 760)
Emission wavelength	1047 nm	1054 nm
Gain bandwidth	1.3 nm	20 nm
Emission cross section	1.8×10^{-19} cm^2	0.4×10^{-19} cm^2
Gain saturation fluence	0.5 J/cm^2	2.24 J/cm^2
Upper-state lifetime	480 μs	360 μs
Refractive index	1.477	1.508
Nonlinear refractive index	1.7×10^{-16} cm^2/W	2.8×10^{-16} cm^2/W

[a] The Nd:YLF data are taken from Refs. 19 and 20; the Nd:glass data, from Ref. 21.

tion the diode beam was roughly five times diffraction limited. We focused the pump mode down to a spot radius of 140 μm in the horizontal direction and 14 μm in the vertical direction. The laser mode radii inside the crystal were calculated to be 185 and 130 μm in the horizontal and the vertical directions, respectively. Mode locking was obtained by use of a 50-cm-ROC mirror for focusing on the SESAM. The pulse repetition rate was 49 MHz, which corresponds to a cavity round-trip time of 20.4 ns. All the important cavity parameters are listed in Table 2.

For each cavity setup we performed measurements by using semiconductor saturable absorbers with different saturation fluences and modulation depths. The SESAM's are low-finesse A-FPSA's and differ in terms of the number and thickness of the InGaAs quantum wells and in the absorber recovery times. We used single-quantum-well InGaAs absorber structures of 15- and 25-nm thickness and double-quantum-well structures of 10-nm InGaAs thickness, each separated by a 10-nm transparent GaAs spacer. A schematic structure of the SESAM's is shown in Fig. 4. The bandgap of the absorb-

Table 2. Resonator Parameters for the Different Nd:YLF Laser Setups Calculated by the *ABCD* Matrix Formalism

Pulse repetition rate (MHz)	197	149	145	135	49
Effective laser mode area in the gain medium (cm^2)	1.3×10^{-4}	1×10^{-4}	1×10^{-4}	1.3×10^{-4}	7.5×10^{-4}
Effective laser mode area on the absorber (cm^2)	4.2×10^{-4}	0.5×10^{-4}	1.1×10^{-4}	4.3×10^{-4}	3.4×10^{-4}
ROC of M_3 (cm)	20	10	15	30	50
Cavity design	delta	delta	delta	delta	V

ing semiconductor material was at approximately 1060 nm. SESAM's typically show a bi-temporal impulse response that can be measured in a standard pump–probe experiment. The fast component is of the order of 100 fs and arises from the intraband thermalization of the photogenerated carriers. The slow component originates from interband trapping and recombination processes and is typically of the order of several picoseconds, depending on the growth temperature and the growth method. In Fig. 5 we show the pump–probe curves for the same SESAM, once measured with ~100-fs pulses from a Nd:glass laser at 1060 nm and once measured with 4-ps pulses from the diode-pumped V-cavity Nd:YLF laser. The typical bi-temporal impulse response is visible only with the short excitation pulses. For the long (4-ps) excitation pulse the fast component is not seen because the photogenerated carriers thermalize so fast that the unthermalized initial energy distribution does not contribute significantly to absorption bleaching.

The saturation fluence of a SESAM can be extracted from its nonlinear reflectivity curve. The 1.3 W of mode-locked output power from the diode-pumped V-cavity Nd:YLF laser provided enough pulse energy (as much as 26.5 nJ) to measure $R(F_{P,A})$. The absorber parameters of the SESAM's that we used are listed in Table 3. A detailed description of SESAM's can be found in Refs. 8 and 9.

To systematically check relations (13)–(16) we inserted every SESAM listed in Table 3 into the different Nd:YLF cavity setups (see Table 2) and determined the Q-switching stability limit of cw mode locking by varying the pump power of the lasers. When we increased the pump power starting from the threshold value, the laser first passed the regime of QML and then switched to cw mode locking. If we then reduced the pump power again, the transition to QML occurred at a slightly lower pulse energy. This small hysteresis was within the ~20% accuracy of our experiments. Strictly speaking, the stability limit that corresponds to our theoretical derivation is the one for the transition from cw mode locking to QML, i.e., the lower bound of the hysteresis range, because of the linearized stability analysis for small deviations from the cw mode-locked state of operation.

We monitored the mode of operation of the laser by detecting the laser light that was leaking through a highly reflecting cavity mirror (i.e., M_2) with a fast photodiode. The amplified photodiode signal was sent to a microwave spectrum analyzer and a 400-MHz analog oscilloscope. In the time domain, we observed either a train of pulses with low amplitude fluctuations (cw mode locking) or pulse trains with large amplitude variations (QML; see Fig. 1). The period of these oscillations is of the order of the inverse relaxation oscillation frequency. In the spectral domain, the relaxation oscillations can be visualized on the microwave spectrum analyzer as sidebands to the carrier frequency at the pulse repetition rate or to its harmonics. In the cw mode-locked mode of operation the relaxation oscillation peak is usually 50–70 dB below the carrier, while in the Q-switched mode-locked case the sidebands are much stronger (see Fig. 6).

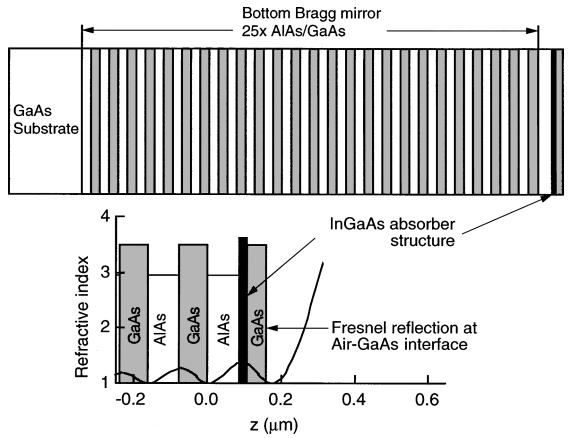

Fig. 4. Schematic structure of the SESAM's. The bottom AlAs/GaAs Bragg mirror is grown by metal-organic chemical-vapor deposition (MOCVD). For the absorber structures we used low-temperature molecular-beam epitaxial or MOCVD growth. The absorber structures consisted of 15- and 25-nm-thick single quantum wells or double quantum wells of 10-nm thickness separated by a 10-nm-thick transparent GaAs spacer layer.

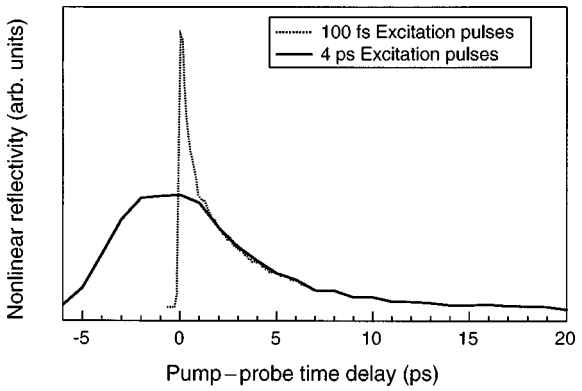

Fig. 5. Measured impulse response of the same SESAM with the use of different excitation pulse durations (100 fs and 4 ps). The fast intraband thermalization (≈200-fs recovery time) is no longer visible with the 4-ps excitation pulse. The slow recovery time is 4 ps.

For the temporal characterization of the laser output in the picosecond to femtosecond regime we used a standard noncollinear autocorrelator. Additionally, we measured the laser spectrum by using an optical spectrum analyzer.

An example of a measurement of the Q-switching stability limit for a cw mode-locked Nd:YLF laser with the

Table 3. Measured SESAM Parameters[a]

Structure (Growth Method)	Saturation Fluence, $F_{\mathrm{sat},A}$ (μJ/cm^2)	Modulation Depth, ΔR (%)	Nonsaturable Loss, ΔR_{ns} (%)	Recovery Time, τ_A (ps)	Symbol
1 QW of 25-nm InGaAs (MBE)	(100±20)	0.9	0.4	4	♦
1 QW of 25-nm InGaAs (MBE)	(80±10)	1.0	0.6	9	◇
2 QW's of 10-nm InGaAs (MBE)	(45± 5)	1.2	0.2	14	□
1 QW of 25-nm InGaAs (MOCVD)	(60±10)	1.7	1.3	26	■
1 QW of 25-nm InGaAs (MBE)	(65±10)	1.3	0.5	40	○
1 QW of 15-nm InGaAs (MOCVD)	(40±10)	0.9	0.5	100	●

[a] QW, quantum well. MBE, molecular beam epitaxy at low temperatures between 350 and 500 °C.

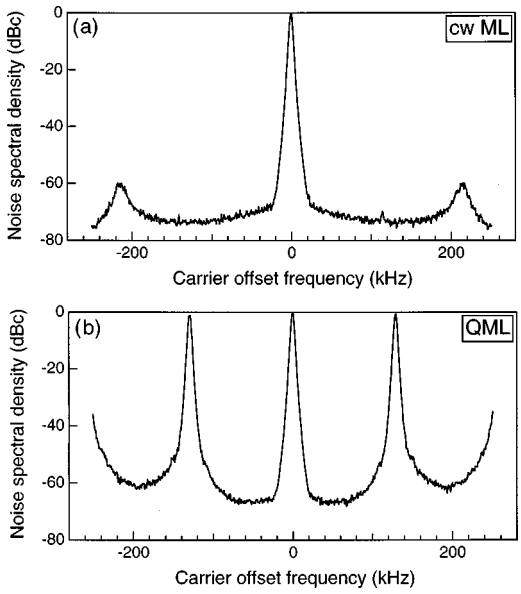

Fig. 6. Microwave spectrum analyzer signal for (a) cw mode locking (cw ML) and for (b) QML of a Nd:YLF laser. The side peaks are due to (a) weak relaxation oscillations and to (b) the large Q-switching modulation, respectively.

MOCVD-grown SESAM with a 15-nm-thick InGaAs absorber is shown in Fig. 7. The measured suppression of the relaxation oscillation peak of the laser below the carrier at the pulse repetition frequency (right-hand ordinate) is displayed versus the pulse energy. At a pulse energy of ≈31 nJ the suppression of the relaxation oscillation peak jumps from a few decibels to more than 50 dB below the carrier, showing the transition from QML to cw mode locking. From Eq. (16) we calculated a critical pulse energy of 29 nJ, using the measured absorber parameters (see Table 3) and the resonator parameters (see Table 2; the ROC of M_3 was 10 cm in this experiment). For further illustration we show the measured nonlinear reflectivity (left-hand ordinate) of the SESAM versus the pulse energy and indicate the stability limit calculated from relation (11). The agreement of relations (11) and (13) with experiment is very good. An assumption in Section 2 was that the absorber relaxation time is long compared with the mode-locked pulse duration; in this experiment we measured a mode-locked pulse duration of approximately 8 ps, which is well below the absorber recovery time of 100 ps.

The experiments with the other SESAM's listed in Table 3 also showed good agreement with theory. The measured pulse durations were between 4 and 10 ps. The measured pulse duration in the QML regime close to the transition to cw mode locking was approximately 40–50% longer than in the cw mode-locked regime. The pulse spectra broadened by approximately the same amount when the laser switched from QML to cw mode locking. The agreement of the experiments with theory was quite good even for the rapidly recovering SESAM's with $\tau_{\mathrm{P}} \approx \tau_{\mathrm{A}}$.

In addition to measuring the stability limits for all the combinations of SESAM's and cavity setups, we also varied the output coupler transmissions (0.5%, 1.5%, and 5%) to verify that the linear cavity loss does not affect the critical intracavity pulse energy. In agreement with the theory we did not observe such an effect.

In Fig. 8 we display the results of all the experiments that were performed. We plotted the critical pulse energy $E_{P,c}$ versus the QML parameter $E_{\mathrm{sat},L}E_{\mathrm{sat},A}\Delta R$ [Eq. (16)]. Above the solid curve with $E_P > E_{P,c}$ the laser is cw mode locked; below that with $E_P < E_{P,c}$ it is Q-switched mode locked. The markers correspond to the experimentally determined stability limits for the different SESAM's and cavity setups. The error bars originate from the uncertainties in the absorber parameters (saturation fluence, modulation depth) and resonator parameters (mode sizes in the gain medium and on the SESAM). We obtained very good agreement between the experiments and theory over a wide parameter range. Note that Fig. 8 contains the experimental results not only for the variation of a single parameter but also for that of a whole set of independent parameters, namely, the laser mode size in the gain medium and on the SESAM's; the SESAM properties ($F_{\mathrm{sat},A}$, ΔR, τ); the pulse repetition rate; and the output coupler transmission. The experiments prove that the QML parameter, which is the product of several independent laser and absorber parameters, is the fundamental quantity that determines the laser dynamics.

B. Femtosecond Regime: Nd:glass

For the femtosecond experiments with the Nd:glass laser we used a standard delta cavity, as shown in Fig. 9. The gain medium is a 4-mm-thick, 4% Nd-doped phosphate glass (Schott LG760) with an absorption length of 0.8 mm at 801 nm. We chose this phosphate glass because it exhibits dominantly homogeneous broadening of its optical

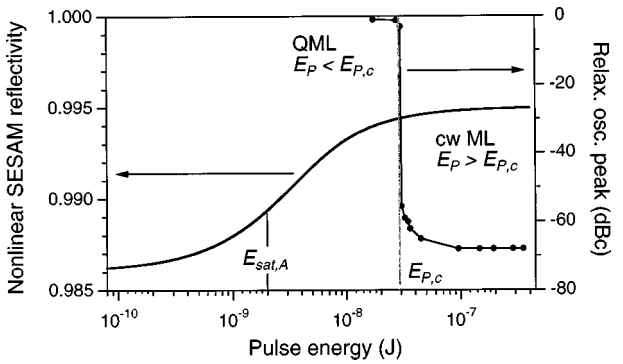

Fig. 7. Experimental determination of the Q-switching stability limit of cw mode locking. The measured suppression of the laser relaxation oscillation peak below the carrier (right-hand ordinate) is displayed versus the pulse energy. The experimentally determined stability limit (≈31 nJ) agrees with the $E_{P,c}$ = 29 nJ calculated from Eq. (16), which is indicated by the vertical line between 10^{-8} and 10^{-7}. For $E_P < E_{P,c}$ we observe QML; for $E_P > E_{P,c}$, cw mode locking. On the left-hand ordinate we show the nonlinear reflectivity of the SESAM.

transitions.[22] We used the same Ti:sapphire pump setup as for the delta cavity experiments with Nd:YLF. The effective laser mode area inside the gain medium was calculated to be $\approx 5 \times 10^{-5}$ cm^2. The laser mode area on the SESAM was calculated to be $\approx 3.7 \times 10^{-5}$ cm^2 for the 15-cm-ROC focusing mirror and $\approx 6.6 \times 10^{-5}$ cm^2 for the 20-cm focusing mirror. The pulse repetition rate of the laser was 75 MHz. To achieve solitonlike femtosecond pulses we introduced an SF10 prism pair for dispersion compensation.[23] We chose a prism separation of 31 cm, which resulted in a total GDD of approximately -2350 fs^2 per round trip.

To check the validity of relations (23) and (27) we used the first two SESAM's listed in Table 3 and the MOCVD-grown SESAM with 25-nm absorber thickness. (In the case of the last two SESAM's listed in Table 3, the absorber relaxation times were not short enough to stabilize a clean femtosecond pulse.) We applied the same procedure as described above to determine the stability limit between QML and cw mode locking.

To evaluate df/dE_P at the stability limit we measured the spectral width $\Delta\nu$ of the mode-locked pulse directly at the transition from QML to cw mode locking and at a slightly increased pulse energy. From these measurements we obtained the increase that occurred in pulse bandwidth $d\Delta\nu$ with increasing pulse energy. We then calculated $df/dE_P = 1/\Delta\nu_g(d\Delta\nu/dE_P)$. We obtained the gain spectrum from the measured fluorescence spectrum of the glass. We fitted the center part of the gain spectrum with a Gaussian spectrum to retrieve the FWHM gain bandwidth $\Delta\nu_g$ to apply the theory described in Subsection 2.D. For the 4% Nd-doped phosphate glass we determined a spectral width of 12.5 nm. This is smaller than the full gain bandwidth listed in Table 1, but it more accurately describes the curvature of the gain spectrum around the center wavelength, which determines the gain filtering effects. df/dE_P varied only slightly from one absorber to the other, which suggests that soliton-shaping effects rather than absorber-related effects dominate. To check this, we compared the measured df/dE_P with the one calculated from Eq. (26), assuming soliton-shaped pulses (D_2 = 2350 fs^2). The values agreed within 15%. Therefore we applied relation (27) to check the theory.

The measured stability limits are shown in Fig. 10. The pulse energy is plotted versus the QML parameter. The dashed curve describes the behavior according to relation (13), i.e., without gain filtering and soliton-shaping effects. The solid curve shows the stability limit according to relation (27), taking into account a GDD of -2350 fs^2. The pulse duration at the transition from QML to cw mode locking was between 400 and 500 fs, and the fraction of the gain bandwidth covered by the mode-locked pulses, f, was between 0.2 and 0.3. The agreement of the measured stability limits with our extended theory is quite good. At lower QML parameters the measured critical pulse energies are somewhat below the calculated values. In these measurements the transition pulse energy from QML to cw mode locking was only approximately twice the absorber saturation energy. Therefore

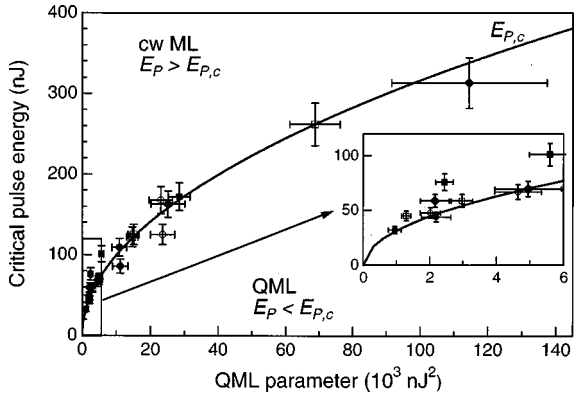

Fig. 8. Results from all the experiments performed to verify relations (13) and (16) for picosecond lasers. The critical pulse energy is shown versus the QML parameter $E_{\mathrm{sat},L}E_{\mathrm{sat},A}\Delta R$. The solid curve shows the theoretical expectation of the critical pulse energy $E_{P,c}$ according to Eq. (16). For higher pulse energies with $E_P > E_{P,c}$, the laser operates cw mode locked; below the solid curve with $E_P < E_{P,c}$ it runs Q-switched mode locked. The markers represent the measured values of $E_{P,c}$ for the different experimental setups and saturable absorbers (compare the markers with the symbols listed in Table 3).

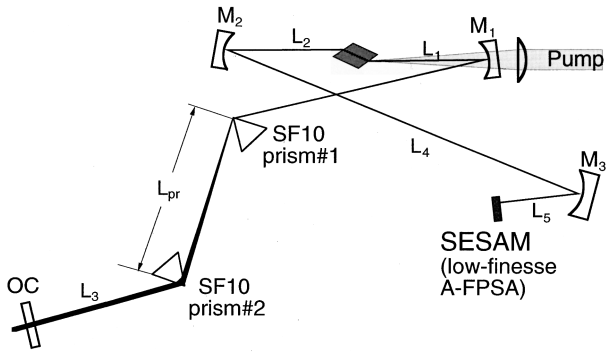

Fig. 9. Nd:glass laser cavity setup. The gain medium is a 4-mm-thick 4% Nd-doped phosphate glass (Schott LG760). The mirrors M_1 and M_2 had a 15-cm ROC, and the lengths were L_1 = 7.6 cm, L_2 = 7.5 cm, L_3 = 100 cm, and L_4 = 75 cm. We used 15-cm- and 20-cm-ROC mirrors as M_3, with corresponding lengths L_5 = 7.4 cm and L_5 = 9.8 cm. The output coupling was 1.5%. The prism separation was L_{pr} = 31 cm.

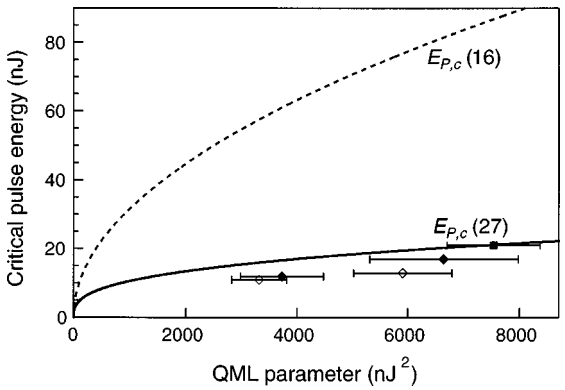

Fig. 10. Q-switching stability limit of cw mode locking for the soliton mode-locked Nd:glass laser. The GDD was approximately -2350 fs^2 per round trip. The dashed curve represents the critical pulse energy $E_{P,c}$ according to Eq. (16); the solid curve takes soliton shaping into account [relation (27)]. Above the curves with $E_P > E_{P,c}$ the laser operation is cw mode locked, below those with $E_P < E_{P,c}$, Q-switched mode locked.

the simplification from Eq. (9) to relations (12) is no longer valid, which results in an overestimation of the critical pulse energy. Another uncertainty with the Nd:glass experiments is some degree of inhomogeneous line broadening. As discussed above, this can reduce the critical pulse energy.

The key conclusion to be drawn from these experiments is that for soliton mode-locked lasers the stability against QML can be significantly higher than predicted by the theory given in Ref. 2 (reviewed in Subsection 2.A). This can be described with good accuracy by our extended model, which takes into account the interplay between soliton effects and gain filtering but neglects possible additional effects caused by the saturable absorber.

4. DISCUSSION

The theory of QML in the picosecond regime, which was confirmed by the good experimental agreement, gives us the handy formula [Eq. (16)] from which we now draw a number of conclusions.

For some applications the development of ultrafast solid-state lasers with high pulse repetition rates in the gigahertz regime is of interest. At higher pulse repetition rates the tendency for QML will increase. In addition, for very short laser cavities we also have to take into account the tendency for pure Q switching,[1,2,9] which is negligible in 100-MHz-type laser oscillators with a saturable absorber recovery time $\tau_A \ll T_R$. Since the pulse energy scales inversely with the pulse repetition rate (for fundamental mode locking and a given intracavity power), a pulse repetition rate that is ten times higher requires an intracavity laser power that is ten times higher, if we leave the QML parameter fixed. At the same pump level, the intracavity power can be increased with reduced output coupling, but only at the expense of efficiency and output power. Typically it is more appropriate to decrease the QML parameter.

We can reduce the absorber modulation depth ΔR by using a thinner absorber layer. However, this leads to longer pulses and to a weaker self-starting tendency of the mode-locking process.[1,2,9]

Tighter focusing onto the SESAM reduces the absorber saturation energy, i.e., $E_{\mathrm{sat},A} = A_{\mathrm{eff},A} F_{\mathrm{sat},A}$. The tradeoffs are that operation of the laser at pulse energies far above the absorber saturation energy can lead to pulse breakup or can damage the SESAM. Investigation of these limitations is not within the scope of this paper. However, in the Nd:YLF experiments with the delta cavity and the 10-cm focusing mirror M_3, we observed the transition from QML to cw mode locking at pulse energies as high as 20–30 times $E_{\mathrm{sat},A}$ without any multiple-pulsing instabilities. Even at increased pulse energies, which resulted in approximately 50 times the absorber saturation energy, we did not reach this limitation. In soliton mode-locked lasers, however, pulse breakup occurs more easily and limits the ratio $E_P/E_{\mathrm{sat},A}$ to values below ≈ 10.[14,18]

Another variable that affects the QML parameter is the gain saturation energy. $E_{\mathrm{sat},L}$ is determined by the gain cross section of the laser material, the laser mode area inside the gain medium, and the type of laser resonator. To minimize the gain saturation energy it is desirable to use a laser material with a large gain cross section, e.g., Nd:YVO_4, rather than Nd:YAG or Nd:YLF. Broadband gain media, suitable for subpicosecond pulse generation, usually have low emission cross sections (with the exception of Ti:sapphire) and thus have a stronger tendency for QML, although, as we have shown, soliton effects can significantly decrease this tendency. Note again that a reduction of the spontaneous lifetime of the upper laser level would not improve the stability of cw mode locking.

The laser mode area inside the gain medium should be chosen to be as small as possible. However, the finite pump mode area is a lower limit because the laser mode area must be somewhat larger than the pump mode area to suppress higher-order transverse modes and to achieve maximum efficiency. Therefore QML can be more difficult to suppress in lasers pumped by high-power laser diodes (with their poor beam quality), while the use of highly doped gain media can be advantageous because the reduced absorption length allows for tighter focusing. Because of their small laser mode areas, waveguide lasers are very interesting for high pulse repetition rates. The gain saturation energy can also be reduced if the pulse passes through the same region of the gain medium several times per round trip.

Under certain conditions an intracavity saturable absorber can support not only fundamental mode locking (with a single pulse inside the resonator) but also harmonic mode locking (with several pulses per cavity round trip), which was demonstrated with a soliton fiber laser.[24] Harmonically mode-locked lasers have a reduced tendency for QML compared with fundamentally mode-locked lasers at the same pulse repetition rate. Generalizing the rate equation analysis described in Section 1 can enable one to derive this. The stability condition from relation (13) for fundamental mode locking changes to

$$N E_P^2 > E_{\mathrm{sat},L} E_{\mathrm{sat},A} \Delta R$$

for harmonic mode locking with N pulses per cavity round trip. For a laser cavity of fixed length L no increase in pump power is required for stable mode locking, if the pulse repetition rate is increased by harmonic mode locking and the mode area on the absorber is adjusted for a constant value of $E_P/E_{\mathrm{sat},A}$. For example, we can double the repetition rate by using twice the value of N and half the value of E_P and $E_{\mathrm{sat},A}$, which reduces both sides of the equation above by a factor of 2 and generates the same average laser power. The limitation of this approach is the heat deposition that is due to the higher average fluence on the saturable absorber.

5. CONCLUSIONS

In this paper we have considered the transition between cw mode locking and Q-switched mode locking in passively mode-locked solid-state lasers with semiconductor saturable absorbers. We have reviewed the previously developed theory by Kärtner *et al.*[2] and have derived simple equations, which has allowed us to calculate the required laser and resonator parameters to achieve cw mode locking without Q-switching instabilities. These calculations agree very well with the results from the experiments that we conducted with picosecond lasers, while femtosecond soliton mode-locked lasers showed a significant reduction of the tendency for Q-switched mode locking. The latter can be qualitatively explained by our extended theory, which takes into account soliton-shaping effects and gain filtering.

ACKNOWLEDGMENTS

We thank J. Hayden from Schott Glass Technologies, Inc., for providing the LG 760 phosphate glass for the femtosecond experiments. This work was supported by a European grant in Biomed 2.

REFERENCES

1. H. A. Haus, "Parameter ranges for cw passive modelocking," IEEE J. Quantum Electron. **12**, 169–176 (1976).
2. F. X. Kärtner, L. R. Brovelli, D. Kopf, M. Kamp, I. Calasso, and U. Keller, "Control of solid-state laser dynamics by semiconductor devices," Opt. Eng. **34**, 2024–2036 (1995).
3. S. Nolte, C. Momma, H. Jacobs, A. Tünnermann, B. N. Chichkov, B. Wellegehausen, and H. Welling, "Ablation of metals by ultrashort laser pulses," J. Opt. Soc. Am. B **14**, 2716–2722 (1997).
4. F. H. Loesel, J. P. Fischer, M. H. Götz, C. Horvarth, T. Juhasz, F. Noack, N. Suhm, and J. F. Bille, "Non-thermal ablation of neural tissue with femtosecond laser pulses," Appl. Phys. B: Photophys. Laser Chem. **66**, 121–128 (1998).
5. H. W. Mocker and R. J. Collins, "Mode competition and self-locking effects in a Q-switched ruby laser," Appl. Phys. Lett. **7**, 270–273 (1965).
6. A. J. DeMaria, D. A. Stetser, and H. Heynau, "Self mode-locking of lasers with saturable absorbers," Appl. Phys. Lett. **8**, 174–176 (1966).
7. U. Keller, D. A. B. Miller, G. D. Boyd, T. H. Chiu, J. F. Ferguson, and M. T. Asom, "Solid-state low-loss intracavity saturable absorber for Nd:YLF lasers: an antiresonant semiconductor Fabry–Perot saturable absorber," Opt. Lett. **17**, 505–507 (1992).
8. U. Keller, K. J. Weingarten, F. X. Kärtner, D. Kopf, B. Braun, I. D. Jung, R. Fluck, C. Hönninger, N. Matuschek, and J. Aus der Au, "Semiconductor saturable absorber mirrors (SESAMs) for femtosecond to nanosecond pulse generation in solid-state lasers," IEEE J. Sel. Topics Quantum Electron. **2**, 435–453 (1996).
9. U. Keller, "Semiconductor nonlinearities for solid-state laser modelocking and Q-switching," in *Nonlinear Optics in Semiconductors*, A. Kost and E. Garmire, eds. (Academic, Boston, Mass., 1998), Vol. 59, Chap. 4, pp. 211–285.
10. B. Braun, K. J. Weingarten, F. X. Kärtner, and U. Keller, "Continuous-wave mode-locked solid-state lasers with enhanced spatial hole-burning. Part I. Experiments," Appl. Phys. B: Photophys. Laser Chem. **61**, 429–437 (1995).
11. F. X. Kärtner, B. Braun, and U. Keller, "Continuous-wave mode-locked solid-state lasers with enhanced spatial hole-burning. Part II. Theory," Appl. Phys. B: Photophys. Laser Chem. **61**, 569–579 (1995).
12. L. M. Frantz and J. S. Nodvik, "Theory of pulse propagation in a laser amplifier," J. Appl. Phys. **34**, 2346–2349 (1963).
13. L. R. Brovelli, U. Keller, and T. H. Chiu, "Design and operation of antiresonant Fabry–Perot saturable semiconductor absorbers for mode-locked solid-state lasers," J. Opt. Soc. Am. B **12**, 311–322 (1995).
14. J. Aus der Au, D. Kopf, F. Morier-Genoud, M. Moser, and U. Keller, "60-fs pulses from a diode-pumped Nd:glass laser," Opt. Lett. **22**, 307–309 (1997).
15. C. Hönninger, F. Morier-Genoud, M. Moser, U. Keller, L. R. Brovelli, and C. Harder, "Efficient and tunable diode-pumped femtosecond Yb:glass lasers," Opt. Lett. **23**, 126–128 (1998).
16. F. X. Kärtner and U. Keller, "Stabilization of soliton-like pulses with a slow saturable absorber," Opt. Lett. **20**, 16–18 (1995).
17. F. X. Kärtner, I. D. Jung, and U. Keller, "Soliton modelocking with saturable absorbers," IEEE J. Sel. Topics Quantum Electron. **2**, 540–556 (1996).
18. F. X. Kärtner, J. Aus der Au, and U. Keller, "Modelocking with slow and fast saturable absorbers—what's the difference?" IEEE J. Sel. Topics Quantum Electron. **4**, 159–168 (1998).
19. P. Peuser and N. P. Schmitt, *Diodengepumpte Festkörperlaser* (Springer-Verlag, Berlin, 1994).
20. D. Milam, M. J. Weber, and A. J. Glass, "Nonlinear refractive index of fluoride crystals," Appl. Phys. Lett. **31**, 822–825 (1977).
21. Schott Glass Technologies, *Laser Glass*, product information (Schott Glass Technologies, Duryea, Pa.).
22. D. Kopf, F. X. Kärtner, K. J. Weingarten, and U. Keller, "Diode-pumped mode-locked Nd:glass lasers with an antiresonant Fabry–Perot saturable absorber," Opt. Lett. **20**, 1169–1171 (1995).
23. R. L. Fork, O. E. Martinez, and J. P. Gordon, "Negative dispersion using pairs of prisms," Opt. Lett. **9**, 150–152 (1984).
24. S. Gray and A. B. Grudinin, "Soliton fiber laser with a hybrid saturable absorber," Opt. Lett. **21**, 207–209 (1996).